nuclear fusion
IAEA

PAPER • OPEN ACCESS

Observation of improved confinement by non-axisymmetric magnetic field in KSTAR

To cite this article: Kimin Kim *et al* 2023 *Nucl. Fusion* **63** 066003

View the article online for updates and enhancements.

You may also like

- Resonant mode effects on rotation braking induced by $n = 1$ resonant magnetic perturbations in the EAST tokamak
H. Sheng, Y.W. Sun, X.Y. Li et al.
- Neoclassical plasma viscosity and transport processes in non-axisymmetric tori
K.C. Shaing, K. Ida and S.A. Sabbagh
- Observation of resonant and non-resonant magnetic braking in the $n = 1$ non-axisymmetric configurations on KSTAR
Kimin Kim, W. Choe, Y. In et al.

This content was downloaded from IP address 1.27.104.22 on 03/11/2023 at 09:50

OPEN ACCESS
IOP Publishing | International Atomic Energy Agency
Nuclear Fusion
Nucl. Fusion **63** (2023) 066003 (8pp)
https://doi.org/10.1088/1741-4326/acc3ad

Observation of improved confinement by non-axisymmetric magnetic field in KSTAR

Kimin Kim[1,*], Jisung Kang[1], Hyunseok Kim[1], Sumin Yi[1], Jeongwon Yoo[2], Minjun Choi[1], Tongnyeol Rhee[1], Junghee Kim[1], Myungwon Lee[2], Won-Ha Ko[1] and Jaemin Kwon[1]

[1] Korea Institute of Fusion Energy, Daejeon 34133, Republic of Korea
[2] Korea Advanced Institute of Science and Technology, Daejeon 34141, Republic of Korea

E-mail: kiminkim@kfe.re.kr

Received 2 February 2023
Accepted for publication 13 March 2023
Published 11 April 2023

Abstract
We report the observation of improved confinement discharge in a magnetic braking experiment in the KSTAR tokamak. The improved confinement is achieved with reduced toroidal plasma rotation by non-axisymmetric magnetic field induced toroidal rotation braking along with significant reduction of edge localized modes (ELMs). Modifications in multi-channel transport raise fast ion slowing-down time and improve neutral beam deposition, leading to improved fast ion confinement. We show that modifications of radial electric field and $E \times B$ shear flow by magnetic braking provoke an enhanced pedestal to sustain thermal confinement against degradation in the typical 3D field experiment.

Keywords: 3D magnetic field, plasma response, magnetic braking, tokamak, improved confinement

(Some figures may appear in colour only in the online journal)

1. Introduction

Development of a high performance operation regime in a magnetic confinement fusion device has been of great interest in the fusion research community for decades as it is critical to maximize fusion power gain in the operation of a fusion reactor. Since the first discovery of high confinement mode (H-mode) in tokamaks that achieved enhancement of energy confinement by more than a factor of 2 compared to low confinement mode (L-mode) [1], a number of advances have been made to expand the territory of high performance operation regimes [2]. Examples of such achievements have been addressed as very high confinement mode (VH-mode) [3], improved H-mode [4], internal transport barrier discharges [5], enhanced pedestal H-mode (EP H-mode) [6], and Super H-mode [7]. These regimes are typically identified by an enhanced transport barrier either or both at the core and edge of plasmas, leading to higher energy confinement than the standard H-mode. Toroidal rotation and shear flow play the key roles in accessing the high performance plasmas [8–10].

It has been widely demonstrated in the present-day tokamak experiments that a non-axisymmetric (3D) magnetic field has the capability to control kinetic and magnetohydrodynamic (MHD) plasma properties [11]. In particular, a number of theoretical analyses [12–14] and experimental observations [15–18] evidence that the 3D magnetic field alters toroidal plasma rotation, called magnetic braking. The impacts of the 3D magnetic field on the toroidal rotation and associated plasma properties have been examined from the control of

* Author to whom any correspondence should be addressed.

Original Content from this work may be used under the terms of the Creative Commons Attribution 4.0 licence. Any further distribution of this work must maintain attribution to the author(s) and the title of the work, journal citation and DOI.

 © 2023 The Author(s). Published on behalf of IAEA by IOP Publishing Ltd

toroidal rotation profile [15, 17, 19, 20] and the Alfvén eigenmode stabilities [21–23]. Confinement degradation has been a typical observation in the 3D field experiment in tokamaks.

In this paper, we report the observation of improved plasma confinement with reduced edge localized modes (ELMs) achieved in 3D magnetic field driven toroidal rotation braking discharges in the KSTAR tokamak. The paper is organized as follows. Section 2 describes the improved confinement of magnetic braking discharges based on the experimental measurements. The impacts of the 3D magnetic field on the fast ion confinement and turbulent transport are discussed in sections 3 and 4, respectively. Discussion is given in section 5.

2. Experimental observations

A dedicated experiment has been conducted in KSTAR, aiming for the control of toroidal plasma rotation utilizing a 3D magnetic field. Time history of the discharges that demonstrate the improved confinement by 3D magnetic field are illustrated in figure 1. The major radius of the plasma is 1.845 m, and the minor radius is 0.47 m. Overall operation parameters are identical for the presented 3 discharges, while the plasma current I_P is varied as 0.6 (black) and 0.7 MA (red, blue) with the fixed toroidal magnetic field $B_T = 1.8$ T. These conditions produced the plasmas with $q_{95} = 3.7$ and 4.5 for $I_P = 0.7$ MA and 0.6 MA, respectively. Neutral beam (NB) heating of 4 MW power was injected in the co-I_P direction in this experiment using three tangential beam sources. The NBs supply strong toroidal torque to generate fast rotating plasmas around 300 km s^{-1} at the plasma axis in the H-mode confinement. The $n = 1$ 3D magnetic field was applied in the plasma current flat-top after the H-mode transition, which drives magnetic braking to modify toroidal rotation profile. The applied 3D field configuration is described in the appendix. As shown in figure 1(a), the 3D field coils were activated at 4.5 s after the H-mode transition, of which currents were ramped up to 4 kA/turn × 2 turns = 8 kA (black, red) or 5 kA/turn × 2 turns = 10 kA (blue) in 200 ms duration. The coil currents were kept constant for 4 s, and turned off at 8.5 s. In addition, we launched the central electron cyclotron heating (ECH) of 1.2 MW in the middle of 3D magnetic field flat-top for further reduction of the toroidal rotation [24]. Therefore, four different phases can be distinguished depending on the combination of NB, 3D magnetic field, and ECH. The NB blips of 1 Hz repetition rate were utilized for charge exchange spectroscopy diagnostics, which caused periodic disturbances to the confined plasmas in the experiment as shown in figures 1, 3, 5 and 6.

One can observe significant reduction of the rotation speed at the center of the plasma in figure 1(b), which is driven by the applied 3D field. This rotation braking globally occurs in the whole plasma volume, as will be shown in figure 2. The toroidal rotation speed is reduced further by the ECH, while the ECH driven rotation reduction is much milder than that driven by the 3D field. Figure 1(c) shows that the 3D field enhances particle transport represented by density pump-out. An interesting finding is that total stored energy from equilibrium

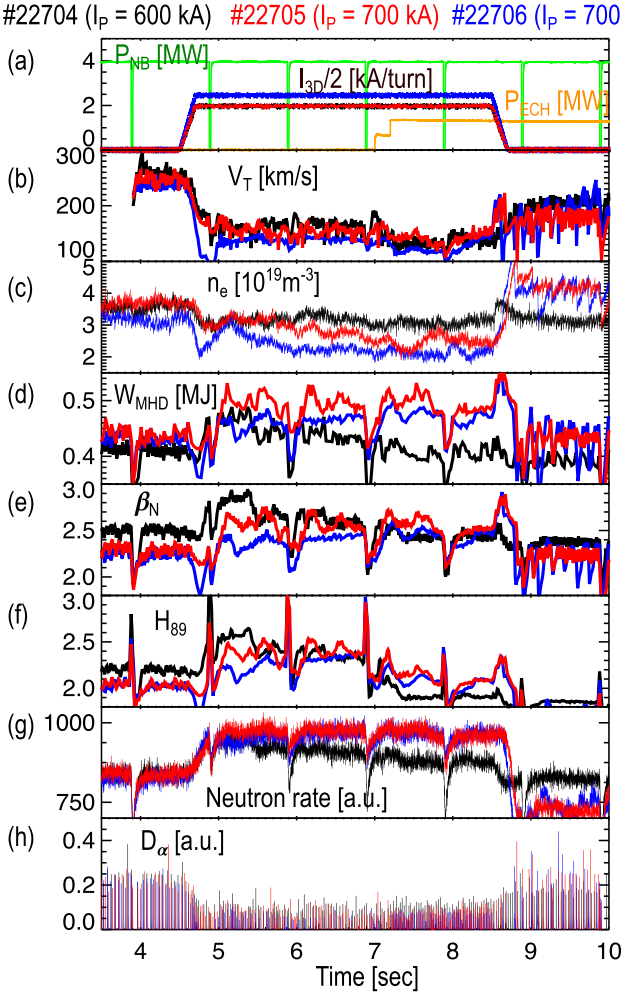


Figure 1. Time history of magnetic braking discharges that achieved improved confinement. (a) Total NB heating power (P_{NB}), 3D coil current (I_{3D}), and ECH power (P_{ECH}), (b) central toroidal rotation speed ($R = 2.0$ (m), (c) line-averaged electron density (n_e), (d) total stored energy (W_{MHD}), (e) β_N, (f) H_{89}, (g) neutron rate, and (h) D_α signal.

reconstruction, W_{MHD} in figure 1(d), is increased by up to 15%–20% in the 3D field phase in spite of the density decrease due to pump-out, indicating improved confinement. Considering typical 3D field experiments for ELM control that lose 10%–20% of confinement, the increment of stored energy is effectively more than 30%. In two discharges of $I_P = 700$ kA (red, blue), the improved confinement is sustained during the whole 3D field period including the latter half with the ECH, while the stored energy is slowly degraded to the level prior to the 3D field application in the $I_P = 600$ kA discharge (black). The normalized confinement quantities β_N and H_{89} are elevated from normal H-mode level to higher lever by 20%. Neutron rates are elevated during the same period under the 3D field for all discharges, implying improved fast ion confinement. Mitigations of ELMs by the 3D field are observed for all discharges as shown by D_α signal. When the 3D field is turned off, the stored energy and neutron rates return to the earlier or even lower levels though the ECH is still on.

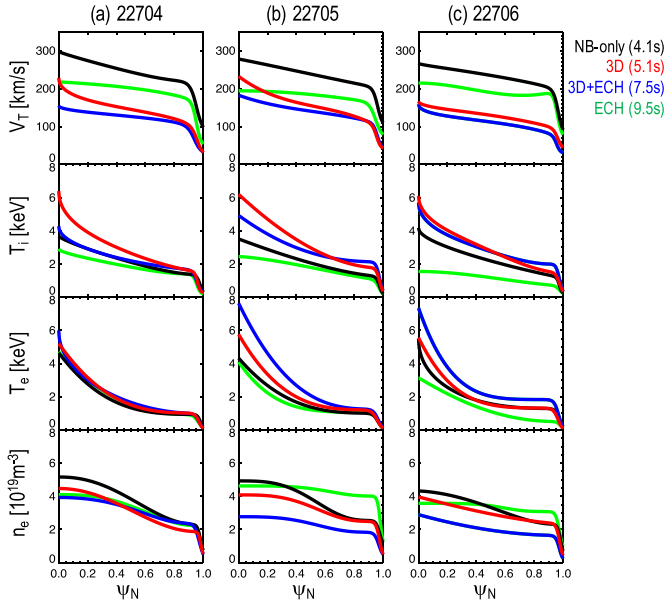


Figure 2. Profiles of toroidal rotation (V_T), ion temperature (T_i), electron temperature (T_e), and electron density (n_e) compared between NB only, 3D field, 3D+ECH, and ECH phases.

This evidences the 3D magnetic field is responsible for the improved confinement.

Kinetic plasma profiles of four separate phases, i.e. NB only, 3D, 3D+ECH, and ECH are compared in figure 2. As previously mentioned, the 3D field induced rotation reduction takes place globally, and thus modify radial rotation profile. This causes modifications of local rotation gradients, which are found to be steeper at the mid-radius region during the 3D and 3D+ECH phases than the NB only and ECH phases. Comparison of ion temperature profiles between four phases indicates that ion thermal confinement is enhanced along with the reduced toroidal rotation during the 3D field period. One notes that build-up of ion temperature profile is correlated to significant reduction of the toroidal rotation, as will be discussed on the multi-channel transport in figure 3. The improved thermal confinement is clearly identified by enhanced edge transport barrier at the pedestal, where the pedestal heights are raised by up to 50%. Electron temperature is also raised by the 3D field, while its increment is milder than ion temperature. The ECH modifies transport channel so that the electron temperature is further raised after the ECH launch, however the ion temperature drops particularly at the core. Plasma temperature is lowered to the normal H-mode level in the ECH only phase, while the density is recovered to even higher level after the 3D field is turned off as observed in the trace of stored energy in figure 1(*d*), where the toroidal rotation profile is recovered to in-between level of NB only and 3D field phases. Such changes in kinetic profiles strongly support that the 3D magnetic field plays the primary role in modifying the plasma confinement in the presented discharges. One notes that plasmas are largely fluctuating in the ECH phase and thereby diagnostic qualities are relatively poor. While it is clear that transport characteristics are quite different in the ECH phase,

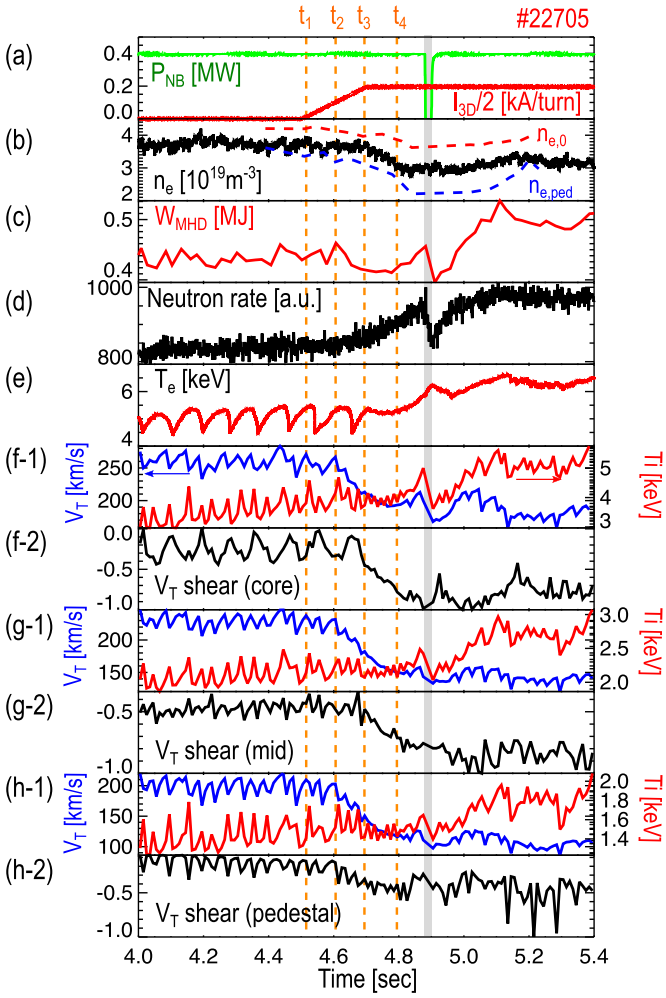


Figure 3. Evolution of kinetic properties in a shorter time scale for #22705. (*a*) Total NB power (P_{NB}) and 3D coil current (I_{3D}), (*b*) line-averaged (n_e), core ($n_{e,0}$), and pedestal ($n_{e,ped}$) electron density, (*c*) total stored energy (W_{MHD}), (*d*) neutron rate, and (*e*) core electron temperature (T_e) are presented. (f,g,h-1) and (f,g,h-2) show evolutions of toroidal rotation (V_T) and ion temperature (T_i), and rotational shear, respectively, at the (*f*) core, (*g*) mid-radius, and (*h*) pedestal. Vertical shade indicates the NB blip period. $n_{e,0}$ and $n_{e,ped}$ in (*b*) are scaled by 0.65 and 1.15 for comparison.

transport analysis due to the ECH launch is beyond the scope of this paper.

Clarifying underlying transport processes, we illustrate the evolution of plasma kinetic properties in a shorter time scale in figure 3. We present the discharge showing the most improved confinement (red, #22705 in figure 1). Other two discharges show similar behaviors in the early improved phase until $t \sim 5.5$ s, however the confinement of discharge #22704 is gradually degraded in the later phase. One finds that the kinetic plasma responses such as density pump-out, rotation reduction, and increase of the stored energy are not promptly initiated by the 3D field application at t_1, but occur in a particular sequence. First, the rotation begins to drop a bit slowly after turning-on of the 3D field coils at t_2, which occurs almost simultaneously in the whole plasma volume. The rotation

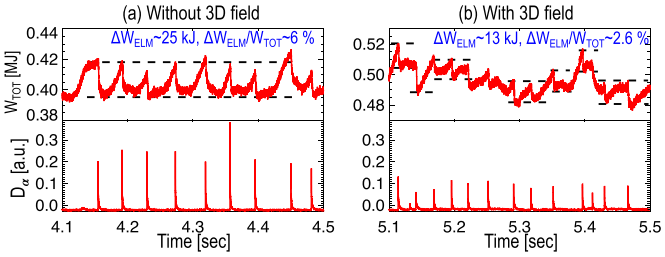


Figure 4. Trace of stored energy W_{TOT} measured by diamagnetic loop along with ELM D_α signal (#22705) (*a*) without and (*b*) with 3D field.

shear build-up begins slightly after the rotation reduction (t_3). The plasma density is observed to be pumped out by the 3D field from edge to core when the 3D field coil currents reach the near-maximum at t_3. It is interesting to note from figure 3(*d*) that the neutron rate slowly begins to rise around t_2 prior to the beginning of 3D field flat-top, and the increase of neutron rate becomes faster around t_3 along with the density decrease. This implies the increase of fast ion contents, which can be related to the increase of the fast ion slowing-down time due to density pump-out and slow increase of electron temperature around t_3. The increase of fast ion population compensates the loss of stored energy by density pump-out, maintaining the total stored energy at a similar level. When the rotation speed reaches the near-minimum level, the ion temperature is raised relatively slowly, and finally the stored energy begins to rise at the time of near-minimum density (t_4). The observed sequential process suggests that the rotation reduction by the 3D magnetic field is the main trigger of the improved confinement. We note that the NB blip near 4.9 s causes instantaneous disturbances, however the confinement is still in the improving state.

Figure 4 illustrates that energy loss by ELMs, ΔW_{ELM} is reduced by about 50% in the improved phase, showing significant reduction of ELM size as $\Delta W_{\mathrm{ELM}}/W_{\mathrm{TOT}} \sim 2.6\%$. This indicates the advantageous feature of the improved confinement discharge that simultaneously achieves higher confinement and much smaller ELMs.

3. Impact on fast ion confinement

The fast ion D-alpha (FIDA) diagnostic [25] confirms that the fast ion confinement is improved throughout the improved confinement phase under the 3D magnetic field. This is illustrated in the time trace of FIDA intensity signal at the core of plasma where $R = 1.89$ m in figure 5. The FIDA intensity is elevated and sustained during the 3D field period, which corresponds to the evolution of stored energy. The ECH injection slightly moderates the FIDA intensity, while the intensity remains higher level than the phase without the 3D field. Turning-off of the 3D field causes a significant drop of the FIDA intensity in spite of the same heating power, which is due to the decrease of fast ion slowing-down time. Changes in the fast ion confinement during the 3D field period are more clearly shown in the FIDA intensity profiles in figure 5(*b*).

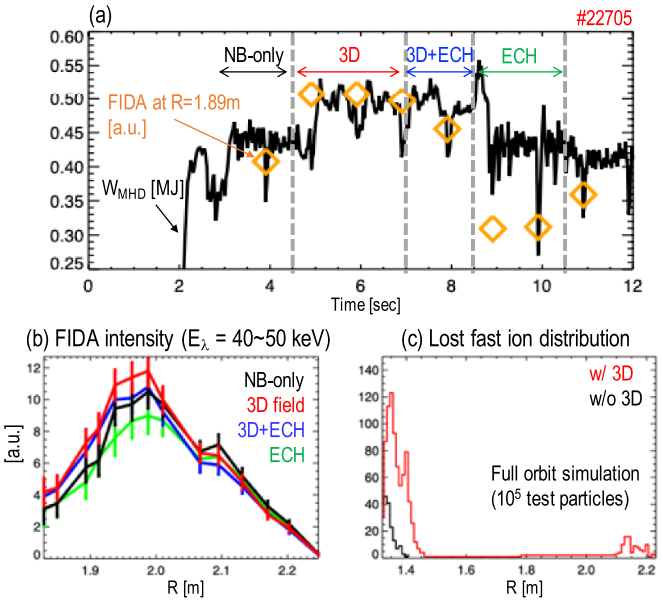


Figure 5. (*a*) FIDA signal overlaid on the evolution of total stored energy (W_{MHD}). (*b*) FIDA intensity profiles compared between four separate phases. (*c*) Distributions of lost fast ions computed by full orbit simulation compared between cases with and without 3D field.

One can find the FIDA intensity is mainly increased at the inner core region of the plasma in the 3D field phase. At the edge, fast ions can be easily pumped out by the 3D magnetic field along with thermal ion pump-out, as will be shown in figure 5(*c*). The ECH degrades the fast ion confinement around the mid-radius where the ECH power is mainly delivered. Removing the 3D field significantly degrades fast ion confinement particularly at the core, which again confirms the main role of the 3D magnetic field.

We performed full orbit particle simulation to examine the fast ion loss driven by the 3D magnetic field for this discharge. We employed the ideal plasma response model using the IPEC code [26] with the kinetic equilibrium (kinetic EFIT) to reconstruct the perturbed magnetic field structure. The beam ion distribution was computed with NuBDeC code [27] using realistic kinetic plasma profiles. Based on those inputs, POCA code [28] was run to simulate the fast ion loss in the presence of a 3D magnetic field. As presented in figure 5(*c*), the full orbit simulation predicts that the applied 3D field causes more beam ion losses compared to the case without the 3D field, which mainly occur at the high field side boundary. This simulation result is contradictory to the FIDA measurement showing the improved fast ion confinement under the 3D field, supporting that the improved fast ion confinement is not caused by the 3D field itself but correlated to modification of kinetic properties such as fast ion slowing down time.

We show in figure 6 that improved fast ion confinement largely contributes to the increase of total stored energy. Thermal stored energy computed with kinetic measurements is found to be temporarily decreased and recovered to slightly higher or similar (red, black), and lower (blue) level compared to the NB-only phase without 3D field. The discharge #22706 shows the largest temporal decrease of thermal stored

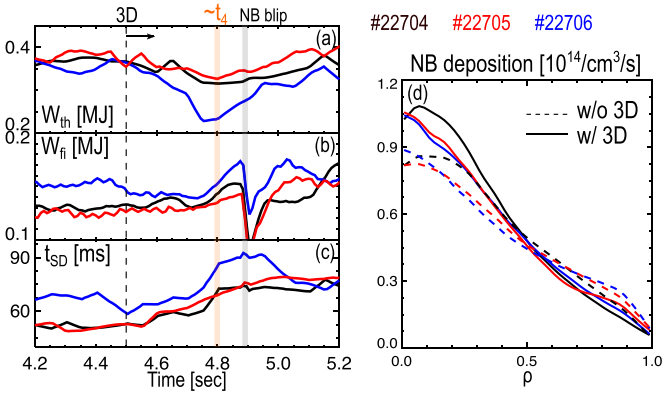


Figure 6. Trace of (*a*) thermal stored energy, (*b*) fast ion stored energy, and (*c*) slowing-down time. (*d*) NB deposition profiles with and without 3D field.

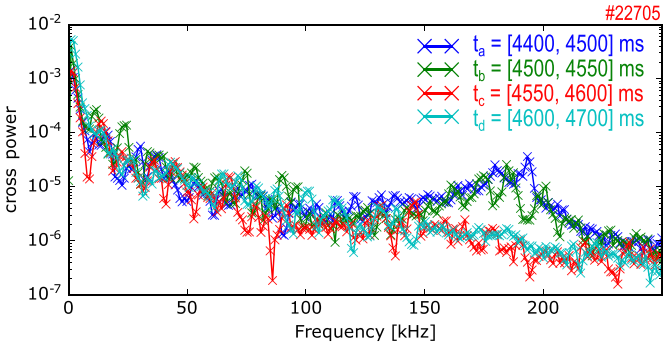


Figure 7. Comparison of cross power spectra measured by ECEI, averaged for four different time window.

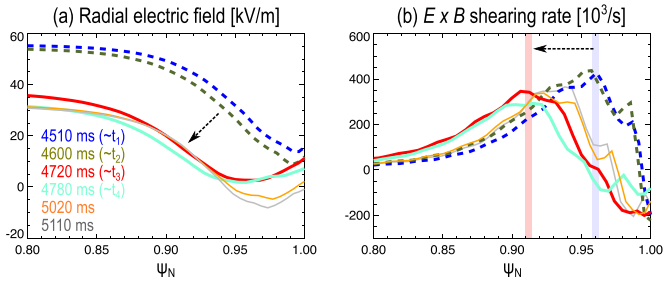


Figure 8. Evolution of (*a*) radial electric field E_r and (*b*) $E \times B$ shearing rate after 3D field application.

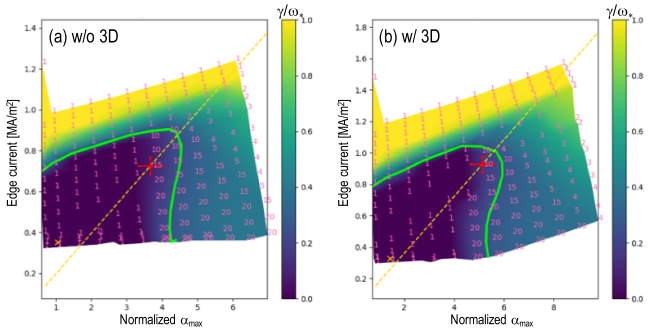


Figure 9. Peeling-ballooning stability diagram (*a*) without and (*b*) with the 3D magnetic field. Green curve indicates the stability boundary defined by $\gamma/\omega_* = 0.25$, where γ is the MHD growth rate and ω_* is the diamagnetic frequency. Red cross indicates the measured pedestal.

energy due to the strongest density pump-out. Fast ion stored energy, computed with TRANSP based on classical transport, is found to be increased by 3D field, which exceeds the thermal loss by density pump-out to increase the total stored energy. This is closely related to longer fast ion slowing-down time and improved NB deposition in the improved confinement phase.

4. Impact on turbulent transport

We find modification of turbulent transport is correlated to the enhanced pedestal. Figure 7 presents the cross power spectra measured by the electron cyclotron emission imaging (ECEI) diagnostic [29] at $R \sim 2.15$ m near the pedestal top. Spectra for four time windows spanning the beginning of 3D field application are compared. One finds that high frequency turbulent fluctuations of 150–200 kHz, that are composed of quasi-coherent modes and broadband fluctuations, exist before (blue, t_a) and slightly after the 3D field is applied (green, t_b). These turbulent fluctuations are active during the former half of the 3D field ramp-up (t_b), however, they are largely reduced or suppressed during the latter half of the ramp-up (red, t_c), indicating the turbulent fluctuations were modified during this 50 ms period. This observation is consistent to the toroidal flow reduction that begins at $t_2 \sim 4.6$ s in figure 3. One can imply that in the middle of 3D field ramp-up, rotations begin to drop to almost simultaneously regulate the high frequency turbulent transport, which leads to the enhanced pedestal. The reduced fluctuations persist during the improved confinement phase under the 3D magnetic field.

We further detail the mechanism of the enhanced pedestal from evolution of the radial electric field E_r and $E \times B$ shearing rate at the edge in figure 8. The E_r is significantly reduced after the beginning of rotation reduction at $t = 4600$ ms ($\sim t_2$ in figure 3), where the rotation braking dominates the E_r evolution. It should be noted that the peak of $E \times B$ shearing rate penetrates toward the pedestal top along with the rotation braking (red) where the pressure gradient is mild, pointing out stronger regulation of the turbulent transport. This is consistent to the ECEI measurement showing the suppression of turbulent fluctuation near the pedestal during the improved confinement phase. Based on these analyses, we suggest that the reduction of toroidal rotation and modification of rotational shear by the 3D magnetic field enhance and raise the pedestal through transport regulation by E_r and $E \times B$ shear flow to raise the plasma temperature in the whole volume.

To better understand the underlying mechanism of the enhanced pedestal in the improved confinement phase, we perform the peeling-ballooning stability analysis using the MISHIKA code [30] with consideration of bootstrap current by Sauter model [31] and diamagnetic stabilization effect. Figure 9 shows the modification of peeling-ballooning stability diagram in the improved confinement phase with 3D magnetic field. The stability analysis indicates the

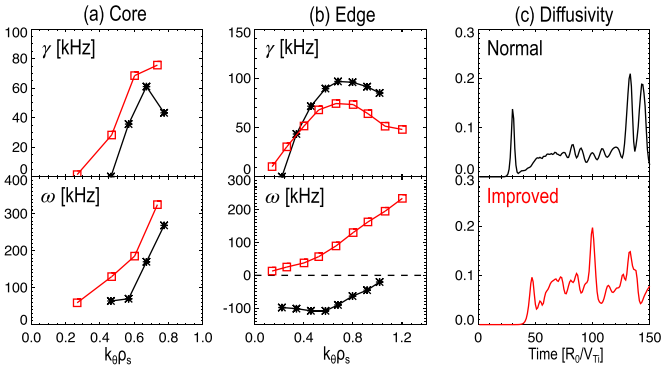


Figure 10. Linear growth rate and mode frequency of normal (black) and improved (red) phase at the (*a*) core and (*b*) edge. (*c*) Nonlinear heat diffusivity (χ_i/χ_{gB}) by gKPSP.

peeling-ballooning stability boundary is extended with the enhanced pedestal. This implies the pedestal in the improved phase was not solely determined by the MHD limit but enhanced by turbulence regulation within the stability margin to the MHD limit after 3D field application.

Global gyrokinetic simulation using gKPSP code [32] with the realistic kinetic profiles compares characteristics of turbulent transport between two cases of normal H-mode before 3D field and improved confinement phase. The purpose of gyrokinetic simulation is to investigate the characteristics of turbulence and to access the possibility of turbulence suppression in the improved confinement phase. The $E \times B$ shear effect is not included in the present simulations. As shown in figure 10, two distinct linear modes are found at the core and edge for the normal phase, which are the ion temperature gradient (ITG) corresponding to $\omega > 0$ and trapped electron mode (TEM) with $\omega < 0$, respectively. As the ion temperature increases in the improved phase, the core ITG mode becomes more unstable. On the other hand, the TEM mode at the edge is found to be converted to the ITG mode, which is stabilized at moderate k but destabilized at low k. The decrease of linear growth rate at the edge in the improved phase can be related to the penetration of the peak $E \times B$ shear shown in figure 8(*b*). One can imply the $E \times B$ flow shear played a role for turbulence suppression in the improved phase. In nonlinear simulations, ion heat transport in the improved phase is found to be larger than the normal phase probably due to destabilization of the low k ITG mode, which is contradictory to the observation of reduced turbulence. Considering fast ion related physics is not included in the gKPSP simulation, fast ion-induced turbulence stabilization [33] may play important roles in improved confinement. Investigations on this topic remain for future study.

5. Discussion

Confinement optimization in the 3D field experiment requires understanding of the origin of different behaviors during the 3D field period observed in three discharges. The plasma response is the key element. As we suggested, the enhanced pedestal and the improved fast ion confinement are the mechanism of the improved confinement in the analyzed magnetic braking experiment. Toroidal rotation reduction is the main driver for the enhanced pedestal, while density reduction and increase of electron temperature are the one for the improved fast ion confinement by increasing fast ion slowing-down time. Crucial differences between the analyzed discharges are the q_{95} value and the applied 3D field strength, which causes distinctive plasma responses to the applied 3D field. They are clearly represented by resonant plasma responses such as strength of density pump-out in this experiment. In the strongest pump-out discharge #22706, temporary loss of thermal stored energy is the largest due to the strongest pump-out and recovered to a slightly lower level than the NB-only phase prior to 3D field application, as shown in figure 6(*a*). The increase of fast ion stored energy exceeds this thermal loss, and leads to increase of total stored energy. On the other hand, the increased total stored energy gradually degrades in the weakest pump-out discharge #22704 in spite of the smallest temporary loss of thermal stored energy by density pump-out. This is probably due to the relatively small increase of the fast ion stored energy, which eventually cannot compensate the thermal confinement loss in the later phase as shown by the neutron rates in figure 1(*g*). The discharge #22705 achieving the largest increase of total stored energy could be in the relatively optimal condition to simultaneously achieve improved thermal confinement with the enhanced pedestal and improved fast ion confinement with the moderate density pump-out. While it is not yet clear enough to draw a conclusion on the optimal condition of the improved confinement, 3D magnetic field configuration that balances strong toroidal rotation braking by non-resonant 3D field components and density pump-out by resonant components may be the key. Investigating the optimal 3D field configuration and plasma conditions will be the important subject to maximize the performance of 3D magnetic field discharge.

In summary, a new confinement improvement mechanism along with ELM mitigation has been observed in the magnetic braking discharges in KSTAR. The observed discharge can be characterized by modification of multiple transport channels driven by 3D magnetic field. They are represented by global rotation braking—momentum transport, density pump-out—particle transport, and enhanced stored energy—thermal transport. Such processes raise fast ion slowing-down time and improve NB deposition, leading to improved fast ion confinement. We suggest modifications of the E_r and $E \times B$ shear flow by the magnetic braking promote build-up of the pedestal to sustain thermal confinement against typical 3D field discharges. This study provides a new opportunity of 3D magnetic field application for high performance operation in magnetic confinement fusion devices.

Acknowledgment

This work was supported by the Ministry of Science and ICT under the KFE R&D program (KFE-EN2341), the ITER Non-procurement Technology R&D Program (KFE-IN2304), and the KSTAR project (KFE-EN2301).

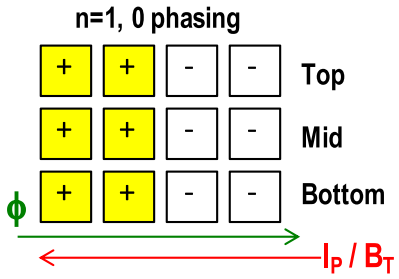


Figure 11. IVCC configuration of $n = 1$, 0-phasing applied in the experiment.

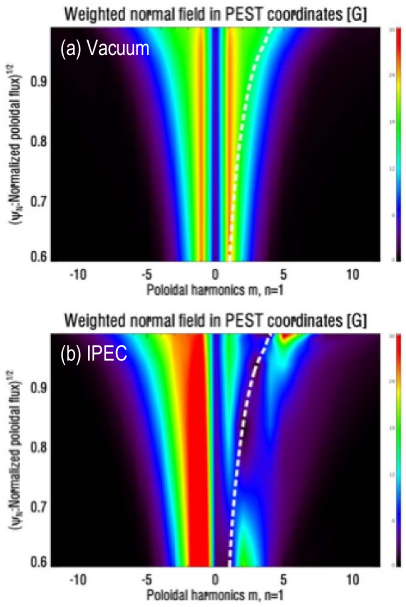


Figure 12. Poloidal field spectrum for #22705 with (*a*) vacuum and (*b*) ideal plasma response. The white dashed line is the locus of the resonant mode $m - nq$.

Appendix. 3D magnetic field configuration

The 3D magnetic field in KSTAR is generated using in-vessel control coils (IVCCs) that have poloidally 3 and toroidally 4 sets of internal coils [34]. The $n = 1$, 0-phasing defined by relative phase differences between three rows is applied in this experiment, of which IVCC configuration is illustrated in figure 11. The poloidal field spectra for #22705 with vacuum field and ideal plasma response computed by the IPEC code are presented in figure 12.

The resonant field and resonant field fraction for the first dominant mode [18, 35] computed with IPEC is compared for three discharges in figure 13. It is indicated the resonant plasma response is the strongest for discharge #22706, where $q_{95} = 3.7$ and the highest IVCC current is applied. The fraction of resonant field is the lowest for discharge #22704 with $q_{95} = 4.5$. The discharge #22705 where the most improved confinement is observed shows moderate resonant plasma responses. Note the resonant field fraction is identical for #22705 and #22706 due to identical q_{95} and 3D

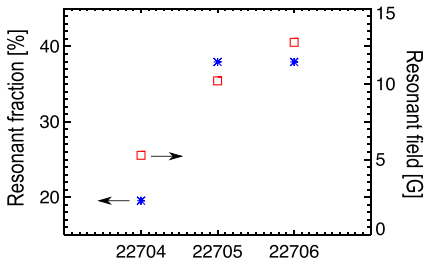


Figure 13. Resonant field and resonant field fraction for the first dominant mode in three discharges, computed with IPEC.

field configuration, while the resonant field is stronger for #22706 due to higher IVCC current. The calculated resonant characteristics are consistent with the observed resonant plasma response such as strength of density pump-out in this experiment.

ORCID iDs

Kimin Kim https://orcid.org/0000-0002-6937-1761
Jisung Kang https://orcid.org/0000-0002-9845-4646
Sumin Yi https://orcid.org/0000-0002-8012-8711
Minjun Choi https://orcid.org/0000-0002-2825-6484
Junghee Kim https://orcid.org/0000-0001-7792-3581

References

[1] Wagner F. *et al* 1982 *Phys. Rev. Lett.* **49** 1408
[2] Wagner F. 2018 *Eur. Phys. J.* H **43** 523
[3] Jackson G.L. *et al* (DIII-D Team) 1991 *Phys. Rev. Lett.* **67** 3098
[4] Gruber O. *et al* (the ASDEX Upgrade Team) 1999 *Phys. Rev. Lett.* **83** 1787
[5] Koide Y. *et al* 1994 *Phys. Rev. Lett.* **72** 3662
[6] Maingi R. *et al* (NSTX team) 2010 *Phys. Rev. Lett.* **105** 135004
[7] Solomon W.M., Snyder P.B., Burrell K.H., Fenstermacher M.E., Garofalo A.M., Grierson B.A., Loarte A., McKee G.R., Nazikian R. and Osborne T.H. 2014 *Phys. Rev. Lett.* **113** 135001
[8] Burrell K.H. 1997 *Phys. Plasmas* **4** 1499
[9] La Haye R.J., Osborne T.H., Rettig C.L., Greenfield C.M., Hyatt A.W. and Scoville J.T. 1995 *Nucl. Fusion* **35** 988
[10] Gerhardt S.P., Canik J.M., Maingi R., Battaglia D., Bell R.E., Guttenfelder W., LeBlanc B.P., Smith D.R., Yuh H. and Sabbagh S. 2014 *Nucl. Fusion* **54** 083021
[11] Callen J.D. 2011 *Nucl. Fusion* **51** 094026
[12] Park J.-K., Boozer A.H. and Menard J.E. 2009 *Phys. Rev. Lett.* **102** 065002
[13] Kim K., Park J.-K., Kramer G.J. and Boozer A.H. 2012 *Phys. Plasmas* **19** 082503
[14] Kim K., Park J.-K. and Boozer A.H. 2013 *Phys. Rev. Lett.* **110** 185004
[15] Park J.-K. *et al* 2013 *Phys. Rev. Lett.* **111** 095002
[16] Kim K., Park J.-K., Boozer A.H., Menard J.E., Gerhardt S.P., Logan N.C., Wang Z.R., Kramer G.J., Burrell K.H. and Garofalo A.M. 2014 *Nucl. Fusion* **54** 073014
[17] Kim K. *et al* 2017 *Nucl. Fusion* **57** 036014
[18] Kim K. *et al* 2017 *Nucl. Fusion* **57** 126035
[19] Garofalo A.M. *et al* 2009 *Phys. Plasmas* **16** 056119
[20] Logan N.C., Park J.-K., Paz-Soldan C., Lanctot M.J., Smith S.P. and Burrell K.H. 2016 *Nucl. Fusion* **56** 036008

[21] Bortolon A., Heidbrink W.W., Kramer G.J., Park J.-K., Fredrickson E.D., Lore J.D. and Podesta M. 2013 *Phys. Rev. Lett.* **110** 265008
[22] Garcia-Munoz M. *et al* (the AUG and MST1 Teams) 2019 *Plasma Phys. Control. Fusion* **61** 054007
[23] Kim K., Kang J., Kim H. and Kim J. 2020 *Nucl. Fusion* **60** 126012
[24] Seol J. *et al* 2012 *Phys. Rev. Lett.* **109** 195003
[25] Yoo J.W. *et al* 2021 *Rev. Sci. Instrum.* **92** 043504
[26] Park J.-K., Boozer A.H. and Glasser A.H. 2007 *Phys. Plasmas* **14** 052110
[27] Rhee T. *et al* 2019 *Phys. Plasmas* **26** 112504
[28] Kim K., Jhang H., Kim J. and Rhee T. 2018 *Phys. Plasmas* **25** 122511
[29] Yun G.S. *et al* 2014 *Rev. Sci. Instrum.* **85** 11D820
[30] Mikhailovskii A., Huysmans G.T., Kerner W.O. and Sharapov S. 1997 *Plasma Phys. Rep.* **23** 844
[31] Sauter O., Angioni C. and Lin-Liu Y. 1999 *Phys. Plasmas* **6** 2834
[32] Kwon J.M., Yi S., Rhee T., Diamond P.H., Miki K., Hahm T.S., Kim J.Y., Gürcan O.D. and McDevitt C. 2012 *Nucl. Fusion* **52** 013004
[33] Di Siena A., Görler T., Poli E., Bañón Navarro A., Biancalani A. and Jenko F. 2019 *Nucl. Fusion* **59** 124001
[34] Kim H.K., Yang H.L., Kim G.H., Kim J.-Y., Jhang H., Bak J.S. and Lee G.S. 2009 *Fusion Eng. Des.* **84** 1029
[35] Park J.-K., Schaffer M.J., La Haye R.J., Scoville T.J. and Menard J.E. 2011 *Nucl. Fusion* **51** 023003